Design and analysis of a composite beam for infrastructure applications

Part III: Experimental results and nonlinear FE analysis

By

Mario Springolo[1], Amar Khennane[2*], Gerard van Erp[3]

[1,2] Faculty of Engineering and Surveying, The University of Southern Queensland, Toowoomba, Qld 4350, Australia

[3] Professor, Executive Director, Fibre Composite Design and Development Centre. The University of Southern Queensland, Toowoomba, Qld 4350, Australia

Abstract:

Using the analytical approaches developed, the cross section of the new fibre composite beam described in the prequels to this paper is designed in order to avert secondary failure modes. A series of specimens have been built and put through a thorough testing regime to establish the performance of the beam. To gain confidence in the analytical models and achieve further understanding of the beam behaviour, a rigorous nonlinear finite element analysis is also presented. It was found that the analytical model agreed relatively well with the experiment and the FE analysis, thus validating the underlying assumptions.

Keywords: composite beam, nonlinear finite element, Abaqus, Python, bending, shear, moment shear interaction

*Lecturer, Faculty of Engineering and Surveying, The University of Southern Queensland, Toowoomba, Qld 4350, Australia
Tel: (+61) (7) 4631 1383, Fax: (+61) (7) 4631 2526, email: khennane@usq.edu.au

Biographical notes: Mr Mario Springolo has submitted his PhD to the Faculty of Engineering and Surveying at USQ. He is currently working as a structural engineer with Larken Teys consulting Pty Ltd. http://www.larkinteys.com.au

Biographical notes: Dr Amar Khennane holds a BE from Tizi-Ouzou, Algeria, an M.Sc. from Heriot Watt, UK, and a PhD, from UQ, Australia. Before joining the Faculty of Engineering and Surveying at the University of Southern Queensland, he was a researcher with the Cooperative Research Centre for Advanced Composite Structures, Ltd, Australia. His research interests are in composite materials: micro-mechanics, durability and through life estimation of composite structures, and computational mechanics.

Biographical notes: Professor Van Erp was born and educated in the Netherlands and moved to Asutralia in 1989. In 1990 he joined the Faculty of Engineering and Surveying at USQ. Currently, he is the Executive Director of Fibre Composites Design & Development, University of Southern Queensland (USQ) responsible of Australia's first fibre composites bridge.

INTRODUCTION

The new fibre composite beam described in the prequels is put through a testing program that includes tests designed for primary and secondary failure modes. In particular, the behaviours in bending, shear, combined bending and shear, buckling, and lateral torsional buckling were investigated. A detailed description of the experimental set up and the complete results are given in [1], and only the most important results are reported herein.

In particular, it was found that the core material cracks prior to the ultimate failure of the beam. This was caused by the low failure strain of 0.6% of the core when compared to the main unidirectional laminates, which have a failure strain around 2%. Associated with the cracking of the core is localised de-bonding at the interface between the laminates and core. In addition, it was found that the different constituents of the beam exhibited different behaviours in tension and compression. The FRP laminates were found to undergo progressive damage due to matrix cracking, fibre-matrix de-bonding and fibre breakage before failure. The best approach to model these phenomena appears to be at micro-mechanical level. However, such an analysis is impossible for large components such as structural elements. Previously some research efforts have assumed equivalent homogeneity to make limited progress. In the present paper, instead of ignoring the lack of homogeneity, attention will be focussed on the internal structure of the material, since it is the latter that governs the behaviour of the composite system and consequently its failure. The approach favoured herein considers the damage progression in the constituents.

Using both the scripting ability of the ABAQUS finite element software [9], and user defined subroutines, the damage phenomena are incorporated in the form of damage variables to

model the nonlinear behaviour of an FRP beam. The obtained results will be compared to both the analytical and experimental results.

FINITE ELEMENT ANALYSIS

Modelling the FRP beam using ABAQUS

ABAQUS is a general finite element package with non-linear capabilities. In particular, whenever a material definition is not supported, the user is provided with the ability to use external subroutines. Taking advantage of the ability to script within ABAQUS, using the Python language [10], an algorithm taking into account the progressive damage within the constituents is proposed. To account for the different material properties in tension and compression, a linear elastic analysis with homogeneous properties is first run to identify stress states within the beam. Material properties are then assigned correspondingly. Because of changes in the model, caused by modelling the damage at different parts of the beam throughout the analysis, this process is updated at each iteration, depending on the stress states obtained at the previous iteration. The cracking in the core material is modelled using a smeared crack approach. When the strain in the core material exceeds a limiting value, the elastic modulus is put to zero at the offending Gauss point. The peel-off of the laminate from the core material is not modelled as the interaction behaviour between core material and laminates is yet to be quantified, and is the subject of continuing investigation. Damage in the laminates is modelled by means of an external Fortran subroutine implementing the damage model of Chang et al. [8]. Furthermore, initial material properties throughout the beam model are varied to imitate the heterogeneous nature of the materials so that stress concentrations may form, providing the sites for crack initiation and laminate failure. A flow chart of the process is shown on Figure 1.

To model the progressive matrix, shear, and compressive failure of the laminates, the existing formulations by Chang et al. [8] were also incorporated within a user defined Fortran subroutine.

PURE BENDING

Finite element model

Figure 2 shows the loading details and the geometrical details of the cross section used to simulate the beam under pure bending. Only the shaded area, pure bending part, shown on Figure 2-a is analysed.

Due to symmetry, only half of the section is analysed as shown on Figure 3 representing the finite element mesh and boundary conditions. The nodes on the left face were constrained to remain on a plane to comply with the Bernoulli hypothesis that plane sections remain plane. The nodes on the right hand cross section are fixed in both the first and third direction but free to move in the third (vertical) direction except for three nodes in the middle of the section that are totally restrained. This is necessary to avoid any rigid body movement of the model. The nodes on the longitudinal face of symmetry are only constrained in the first (transversal) direction.

The loading is applied through a couple as shown on Figure 4 to induce pure bending. The core and longitudinal laminates were discretised using 8 noded brick elements as shown on Figure 5. The RHS laminates were discretised using 4 noded shell elements as shown on Figure 6.

Material properties

Material properties were randomly assigned to the brick and shell elements in the models. The distribution was based upon the average and standard deviation recorded in testing the laminates and the Particulate Filled Resin (PFR) shown in Table 1 of Part I of the prequel. To ensure that results were statistically valid, 30 models, each with a different randomisation sequence, were analysed for each loading configuration. Both the assigning of tensile and compressive properties, and the modelling of progressive failure was achieved within ABAQUS via a user defined Fortran subroutine. The core material cracking and FRP tensile capacities were based on a maximum strain criterion. To simulate the cracked behaviour of an element, the tensile and shear moduli, respectively parallel and perpendicular to the direction of failure, were re-set to one. The 10 different principal strain states possible as represented on Table 1. For example, if a brick element representing a laminate is under a state of tension (T) in the direction of $\varepsilon_{11,}$ and compression (C) in the directions of ε_{22} and ε_{33}, then the tensile modulus E_{11} will be used in the direction of $\varepsilon_{11,}$ while the compressive moduli E_{22} and E_{33} will be used in the directions corresponding to ε_{22} and ε_{33}. Original non-failed value (OV) for Poisson's ratios and shear moduli will also be used. However, if it has already failed in any direction (represented by the letter F), then failed values (FV) for the elastic properties in that direction will be used. Table 1 is used to model the progressive matrix, shear, and compressive failure of the laminates using the damage formulation developed by Chang et al. [8]

Results and discussion

Figure 7 shows the obtained results for the beams tensile and compressive strains at mid-span (denoted T and C respectively in the figure). It can be seen that there exist an excellent

correlation with both the experimental and analytical results. Furthermore, the FEA and analytical ultimate capacity predictions agree very well with the experimental results.

The difference in the analytical and FEA predictions of tensile strains, between moments of 1E6 to 1.75E6 *Nmm* on Figure 7, could be attributed to the fact that the FEA model does not provide for core-laminate de-bonding. Given the current state of knowledge, this de-bonding behaviour cannot be modelled reliably, regardless of the FEA package chosen. As mentioned previously, the characterisation of this phenomenon is still under investigation. However, the FEA results converge to the analytical predictions above a moment of 1.75E6 *Nmm*, which is of prime importance as far as prediction of loading capacity is concerned. To further test the validity of the developed FEA approach a number of models with altered beam geometry are compared against experimental data. As can be seen on Figure 8 to Figure 11, the FEA predictions are consistent for all the beam geometries tested.

MODELS UNDER SPECIFIC LOADING REGIMES

The developed approach provides excellent correlation with analytical and experimental results under a state of pure bending. To establish the overall applicability of the approach, it is used to model the beam behaviour, and predict the occurrence of following range of failure modes:

- moment buckling of the webs,
- combined shear and bending,
- shear buckling of the webs, and
- lateral torsional buckling

Moment buckling of the webs

Testing for web buckling required the manufacture and testing of separate web specimens. These specimens are modelled as per the four-point bending test arrangement. The first buckling mode, as predicted by the model, is shown on Figure 12. Comparison of results, as shown on Table 2, shows that the analytical and finite element solutions are similar and agree well with the experimental results.

Combined shear and bending

Six beams loaded in four-point bending were analysed. Due to symmetry, only half spans were modelled. The lengths of the spans were successively reduced to obtain the interaction diagrams between moment and shear. Figure 13 shows the two extremes of the model geometry's. The obtained failure predictions, together with the analytical and experimental results, are plotted on Figure 14. It can be seen that the FEA results reproduce the trend of the experimental results shown as dots on the plot. However, the FE results correlate with the analytical results only at either high-shear and low moment or low-shear and high-moments. Furthermore, the general trend shown by the FE results seems to follow occurrences of cracking in the core material as experimentally observed.

Shear buckling of the webs

To model shear buckling, a web specimen similar to that used to test for moment buckling, was modelled. The first predicted buckling mode is shown on Figure 15. As with moment buckling, comparison of the results, as reported on Table 3, shows good agreement between the analytical, FE and experimental results.

Lateral torsional buckling

In line with the experimental set up, a two-meter long cantilevered beam was modelled. The model was solved to obtain the eigenvalues. Figure 16 shows the first predicted buckling mode. As shown on Figure 17, there is some variability between the experimental, theoretical and FEA results. The Eurocomp formulation for FRP beams is substantially lower than the other methods. The remainder of the predictions lie within 27% of each other. The FEA is within 11% of the critical moment as observed in the experimentation.

CONCLUSIONS

The behaviour of the developed beam has been well described using advanced nonlinear finite element analysis that incorporates heterogeneous material property description and damage progression in the individual constituents of the beam. In particular, the developed FE approach captured the interaction between shear and bending better than any other method

Both the experimental results and the non linear finite element analysis corroborated that the addition of the core material to the flanges and webs of the newly developed beam suppresses most of the premature failures modes known to occur in existing designs. This constitutes an improvement in overall beam performance. However, it was also revealed that failures from point loads, and combined moment–shear interaction, are dominated by buckling failure due to the cracking of the core material. Contrary to existing belief, it was found that the pure shear capacity of the web laminates is governed by fibre fracture rather than fibre pull-out as is described in codes and the literature.

The simplified analytical formulas described in the sequels show very good agreement with both the experimental results and FE analysis. These formulas were initially formulated for designing the experimental program. However, in the light of the observed accuracy, these formulas could constitute the basis for designing these FRP beams.

References

1. Springolo, M. New fibre-reinforced polymer box beam: investigation of static behaviour. PhD thesis. Faculty of Engineering, The University of Southern Queensland, Australia. 2005. http://adt.usq.edu.au/adt-QUSQ/public/adt-QUSQ20050421.122411/
2. Ascione L, Feo G, Mancusi G. On the statical behaviour of fibre-reinforced polymer thin-walled beams. Composites Part B: Engineering. 2000; 31B(8): 643-653.
3. Barbero EJ, Lopez-Anido R, Davalos JF. On the mechanics of thin-walled laminated composite beams. Journal of Composite Materials. 1993; 27(8): 806-829.
4. Davalos JF, Qiao P. Analytical and experimental study of lateral distortional buckling of FRP wide-flange beams. Journal of Composites for Construction. 1997; 1(4): 150-159.
5. Davalos JF, Salim P, Qiao R., Lopez-Anido R, Barbero E J. Analysis and design of pultruded FRP shapes under bending. Composites Part B: Engineering. 1996; 27(3/4): 295-306.
6. Haj-Ali R, Kilic H. Nonlinear behavior of pultruded FPR composites. Composites Part B: Engineering. 2002; 33(3):173-191
7. Taufik A, Barrau JJ, Lorin F. Composite Beam Analysis with Arbitrary Cross Section. Composite Structures. 1999; 44(2/3): 189-194.
8. Chang F, Lessard L, Chang K, Liu S. Damage tolerance of laminated composites containing a hole and subjected to tension or compression. 34th International SAMPE

Symposium and Exhibition - Tomorrow's Materials: Today. SAMPE, Covina, CA, USA, 1989 p:559-568.

9. Hibbitt, Karlsson & Sorensen Inc., 'ABAQUS', ver 6.4, Hibbitt, Karlsson & Sorensen, Inc., Pawtucket. RI 02860-4847, USA, 2003

10. Van Rossum G. Python Software Foundation. http://www.python.org/

Table 1: Material properties for failure modelling

Principal strain state C = compression, T = tension, and F = failed in tension			**Material properties** Com. = compression modulus, Ten. = tension modulus, OV = original non-failed value used, and FV = failure value used (1 for E and G, 0 for ν)								
ε_{11}	ε_{22}	ε_{33}	E_{11}	E_{22}	E_{33}	ν_{12}	ν_{13}	ν_{23}	G_{12}	G_{13}	G_{23}
C	C	C	Com.	Com.	Com.	OV	OV	OV	OV	OV	OV
T	C	C	Ten.	Com.	Com.	OV	OV	OV	OV	OV	OV
F	C	C	FV	Com.	Com.	FV	FV	OV	FV	FV	OV
T	T	C	Ten.	Ten.	Com.	OV	OV	OV	OV	OV	OV
F	T	C	FV	Ten.	Com.	FV	FV	OV	FV	FV	OV
F	F	C	FV	FV	Com.	FV	FV	FV	FV	FV	FV
T	T	T	Ten.	Ten.	Ten.	OV	OV	OV	OV	OV	OV
F	T	T	FV	Ten.	Ten.	FV	FV	OV	FV	FV	OV
F	F	T	FV	FV	Ten.	FV	FV	FV	FV	FV	FV
F	F	F	FV	FV	FV	FV	FV	FV	FV	FV	FV

Table 2: Moment buckling of the web specimen

	Analytical	**FEA**	**Experimental**
Buckling moment (10^5 N.mm)	9.66	9.68	Buckled at: 8.60 Failed at: 9.72

Table 3: Shear buckling of the web

	Analytical	**FEA**	**Experimental**
Shear Load (N)	6871	7023	Buckled at: 7500 Failed at: 9370

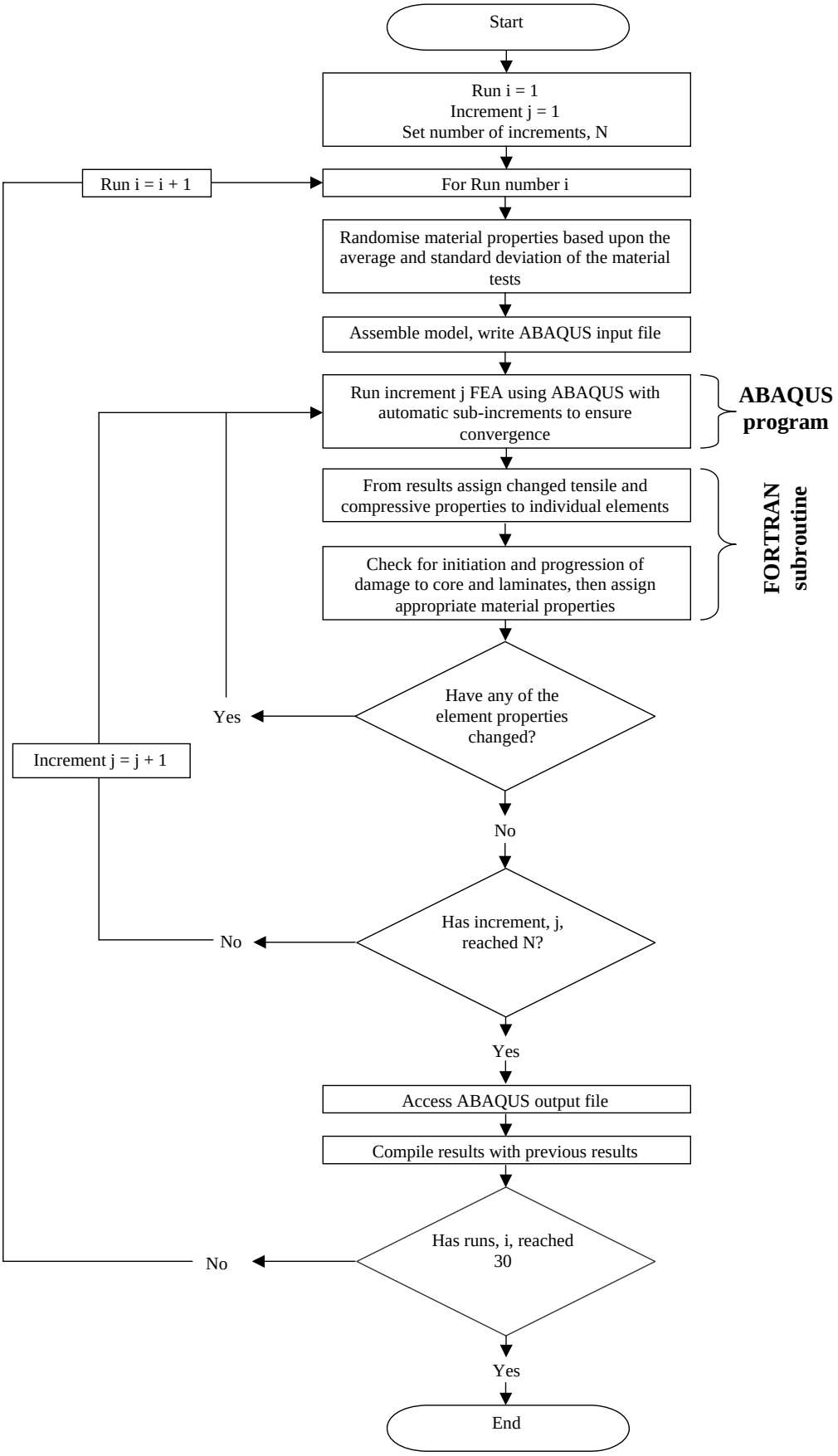

Figure 1: Flow chart of Python script

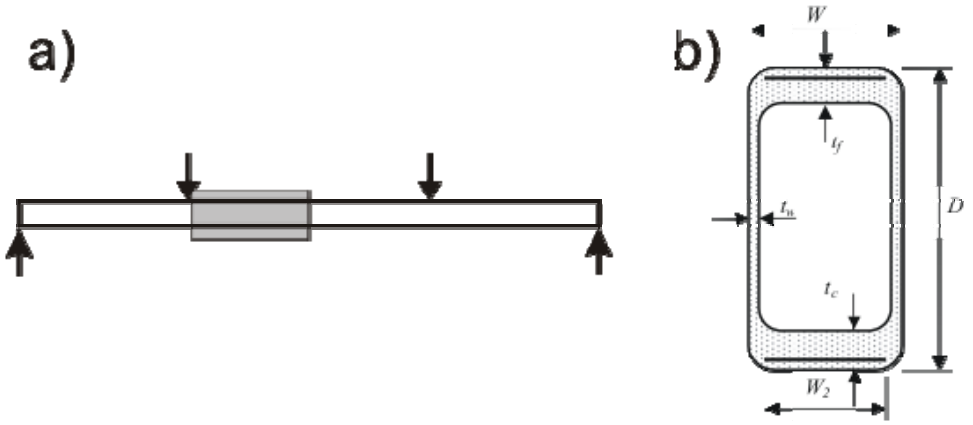

Figure 2: Loading details and cross section .

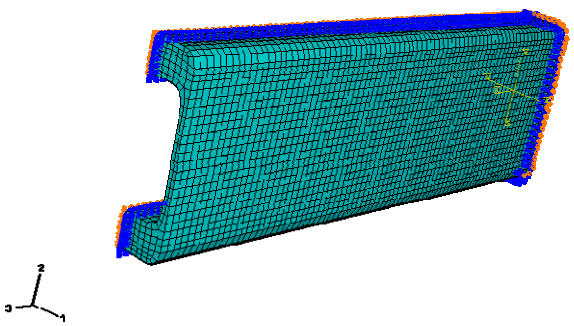

Figure 3: Finite element mesh and boundary conditions for pure bending

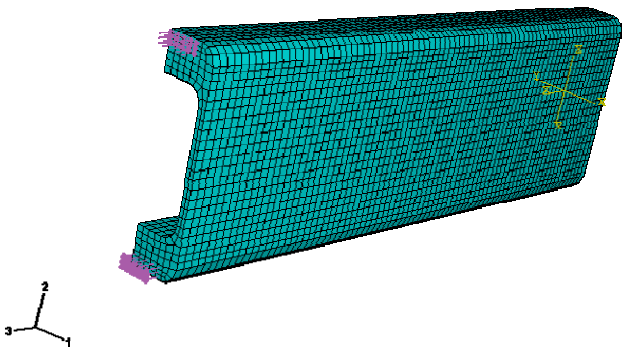

Figure 4: Finite element mesh and loading for pure bending

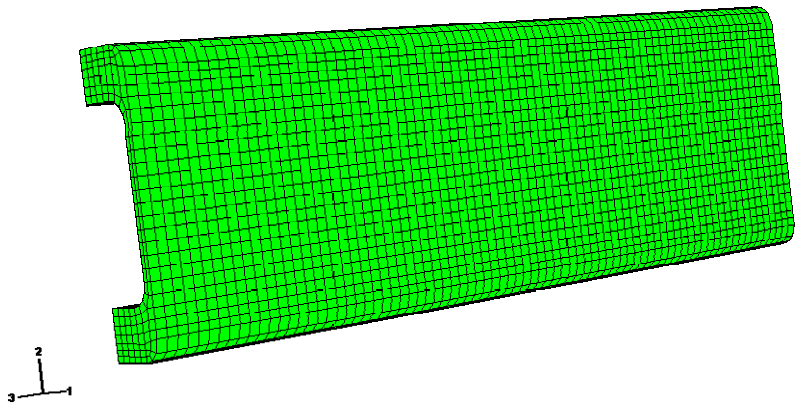

Figure 5: Finite element dicretisation of the core and longitudinal laminates

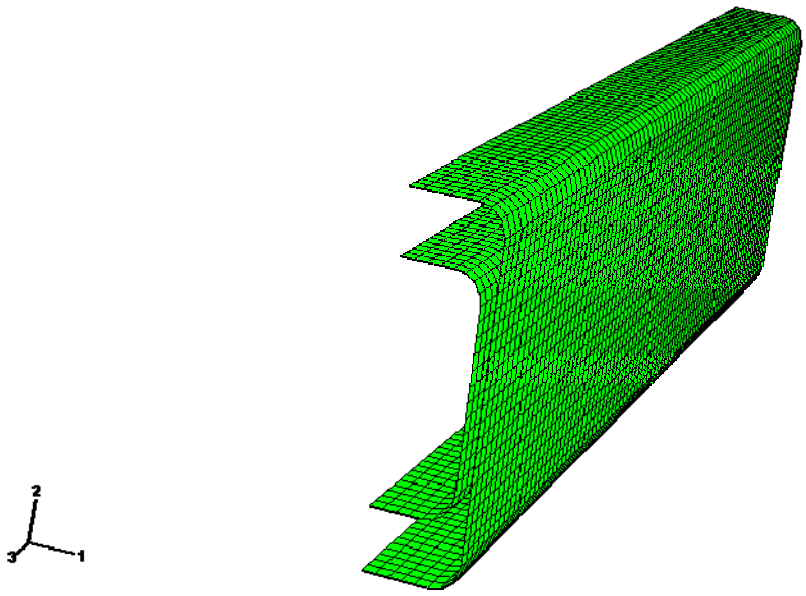

Figure 6: Finite element dicretisation of the RHS laminates

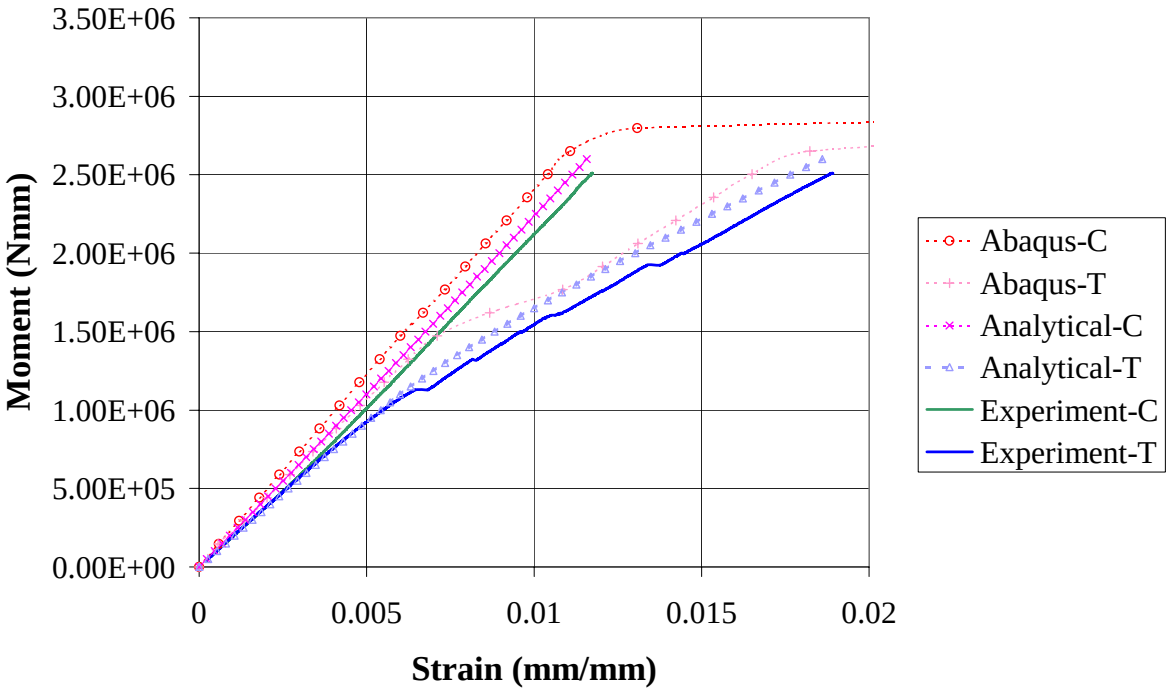

Figure 7: FE models versus analytical and experimental results

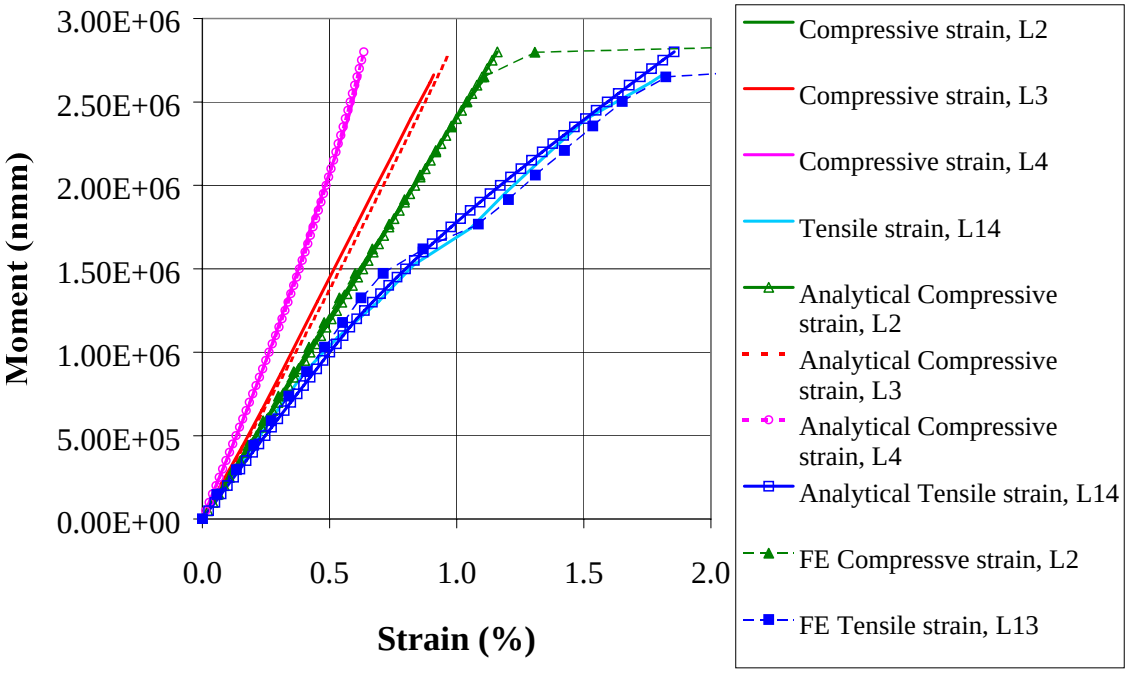

Figure 8: FE versus analytical and experimental results for changing flange core thickness, series B6

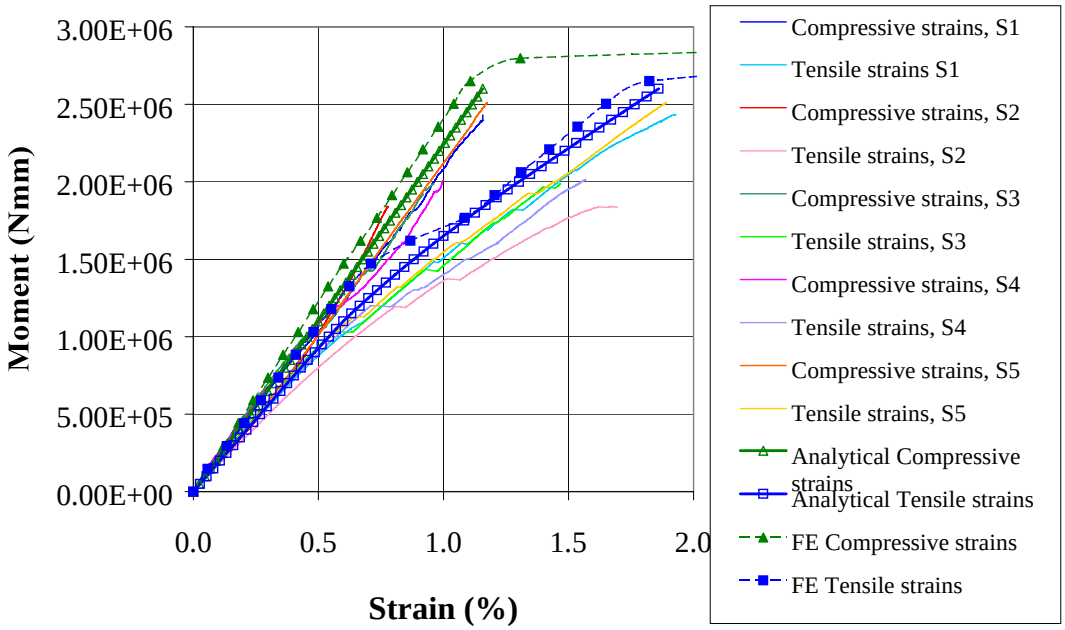

Figure 9: FE versus analytical and experimental results for changing flange core thickness, series B6

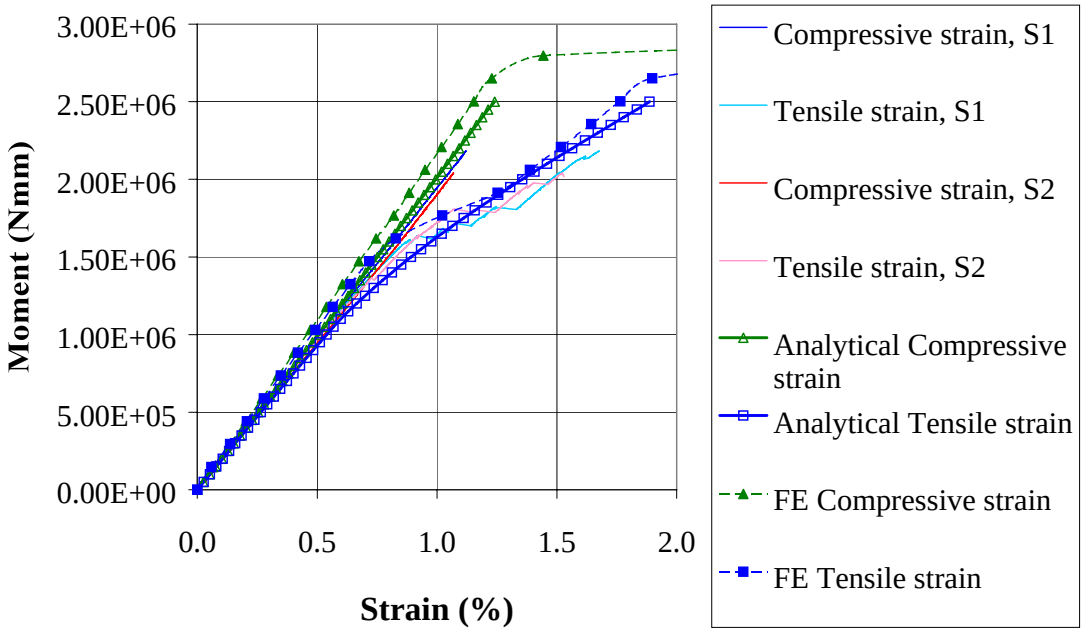

Figure 10: FE versus analytical and experimental results for changing flange core thickness, series B8

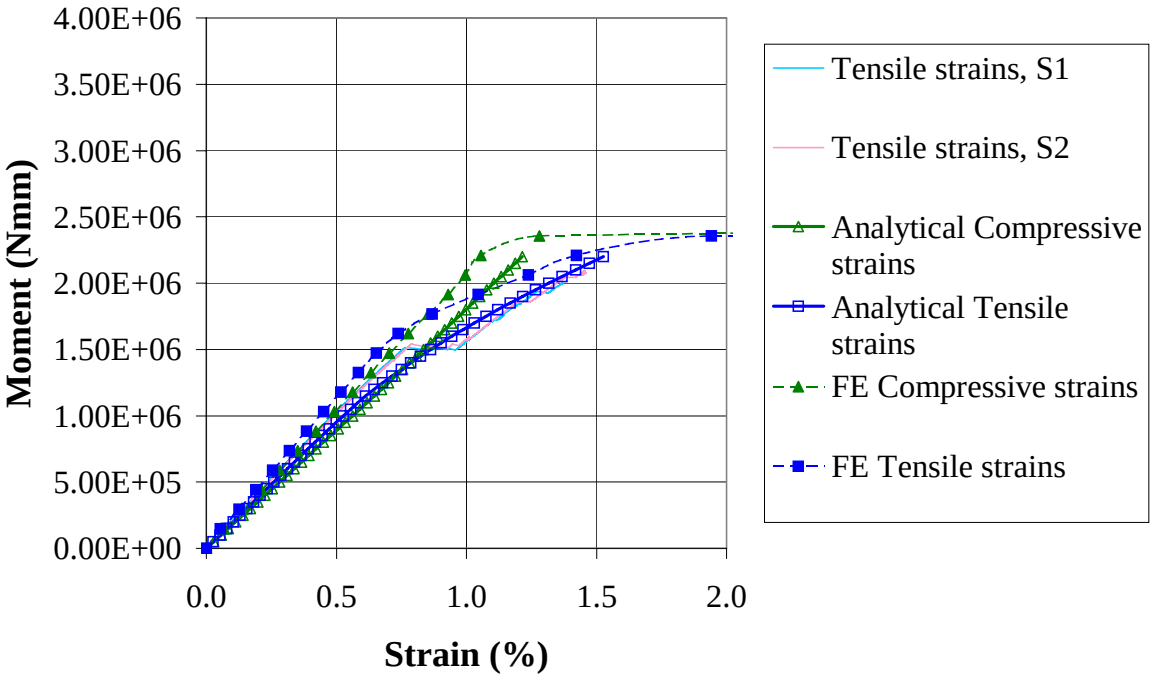

Figure 11: FE versus analytical and experimental results for changing flange core thickness, series B9

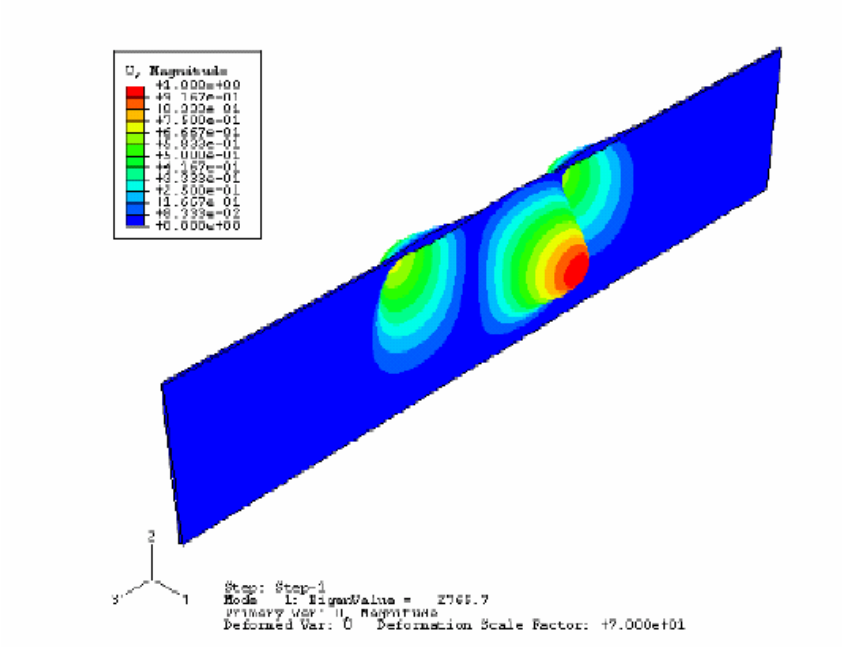

Figure 12: Moment buckling of the web specimen

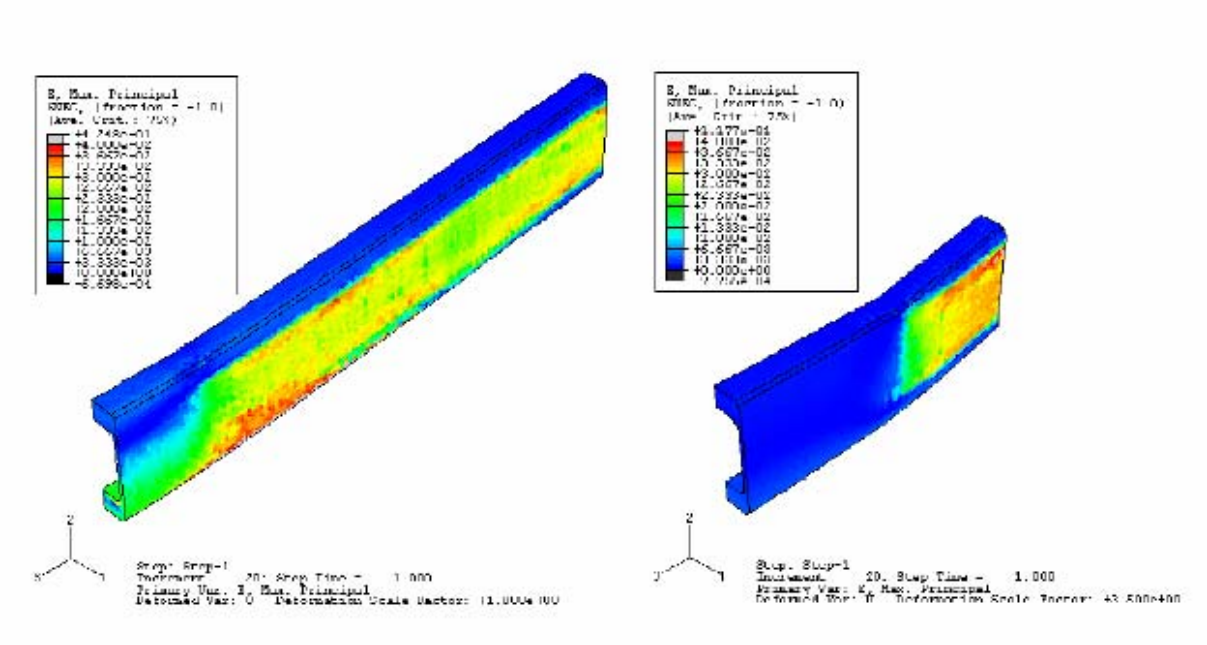

Figure 13: Combined shear and bending.

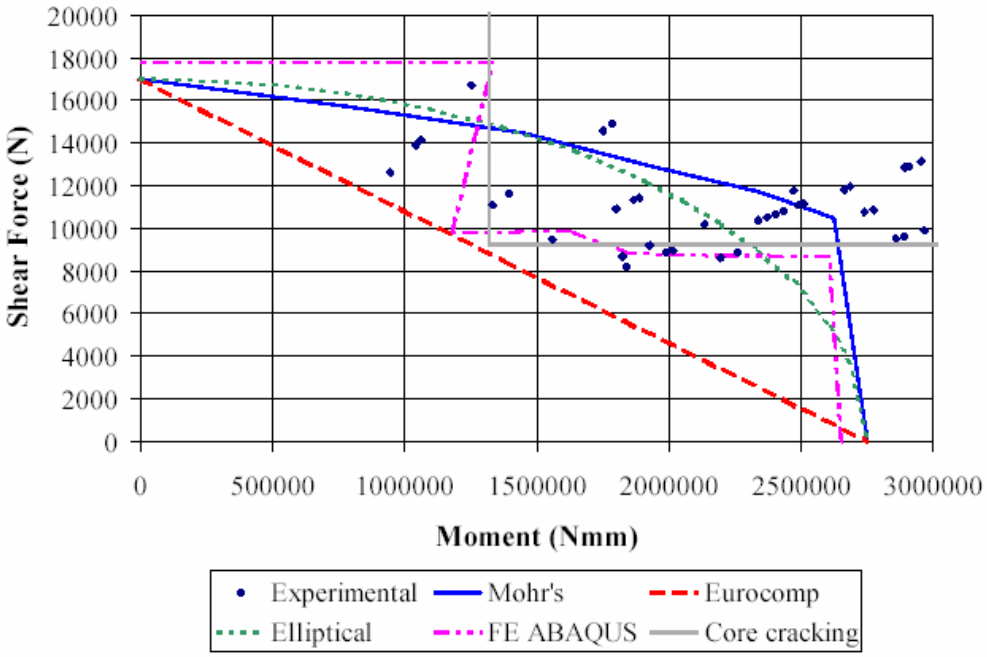

Figure 14: Results for combined shear and bending

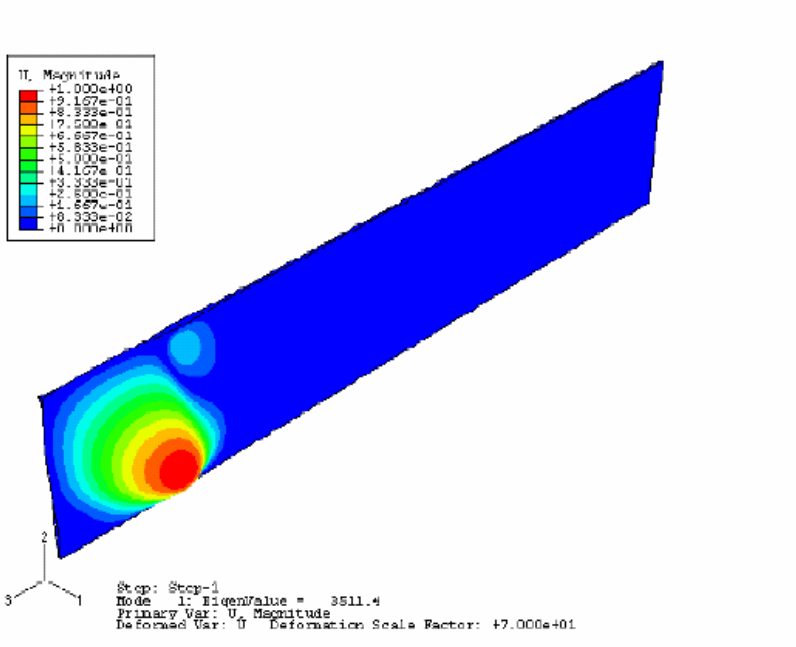

Figure 15: Shear buckling of the web

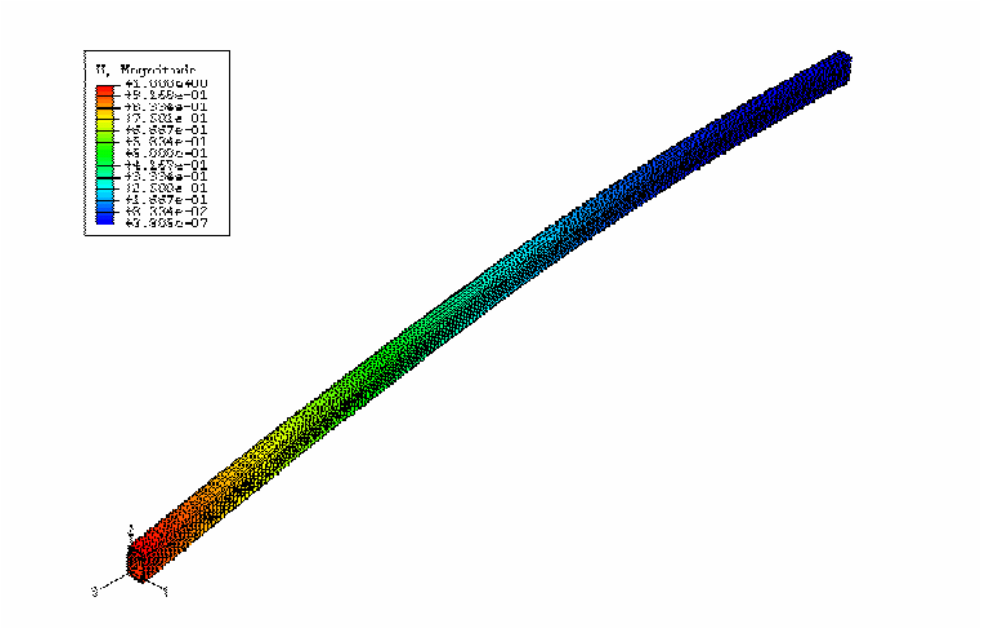

Figure 16: Lateral torsional buckling

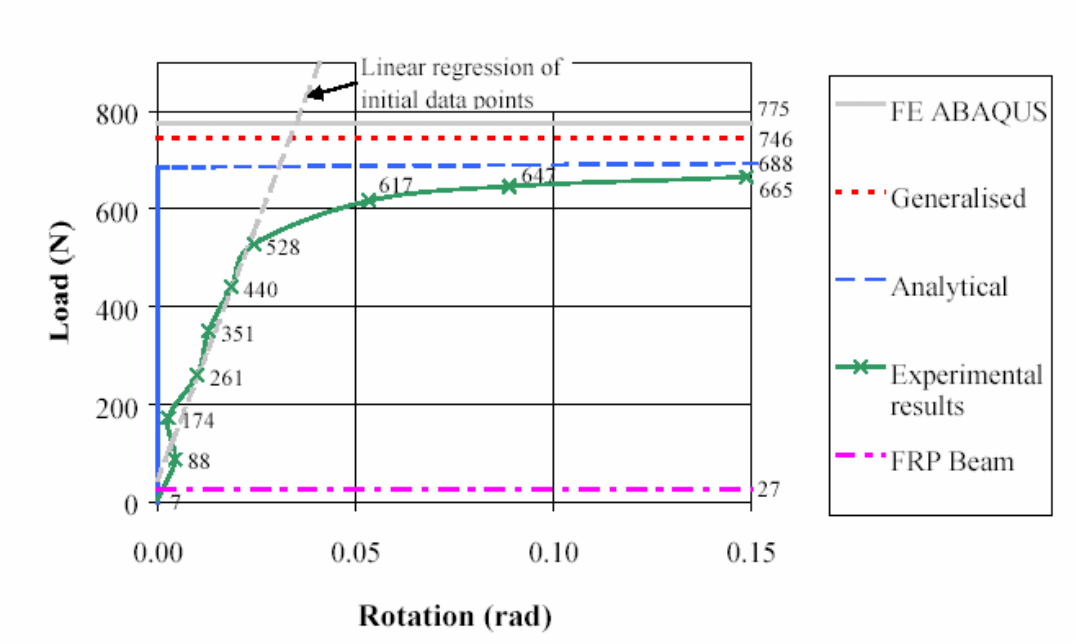

Figure 17: Comparison of lateral torsion buckling predictions